Supporting information Hofmann *et al.*

Materials and Methods

Protein preparation. GroES was expressed in BL21DE3 cells. After cell disruption in 50 mM TrisHCl, 1 mM EDTA, pH 7.5 (buffer A) and centrifugation for 15 min at 4 °C (21000 rpm, F21S50 rotor, Herolab), the supernatant was filtered and loaded on a Q-sepharose column (GE Healthcare Biosciences, Piscataway, NJ) equilibrated with buffer A (1). The column was washed with 500 ml of buffer A before starting a gradient from 0 to 1 M NaCl at a flow rate of 4 ml/min. Fractions containing GroES were combined. After heat precipitation for 20 min at 80°C in the presence of 10 mM EDTA (2), GroES was 80 % pure (according to SDS-PAGE). The remaining impurities were removed by size exclusion chromatography (Sephadex S75 26/60, GE Healthcare Biosciences, Piscataway, NJ) under denaturing conditions (50 mM TrisHCl, 1.5 M GdmCl, 1 mM EDTA, pH 7.5). Finally, the protein was refolded by dialyzing twice against 1 liter of buffer A, frozen in liquid nitrogen, and stored at -80°C. GroEL-SR1 was expressed and purified essentially as described by Horwich *et al.* (3) and stored at -80 °C as a precipitate in 2.7 M ammonium sulfate. Cysteine variants of rhodanese (E77C, D102C, K135C, K174C, D219C, K236C, E285C, E77C/K135C, K135C/K174C, K236C/E285C) were prepared and labeled with Alexa Fluor 488 and Alexa Fluor 594 (Förster radius of 5.4 nm (4-6)) as described previously (6).

We have taken the following measures to minimize the risk of perturbing the refolding kinetics by fluorophore labeling. [1] We selected chromophores with good solubility in water, which showed little or no influence on protein stability and dynamics in previous experiments (4, 7-12). [2] Previous size exclusion chromatography experiments showed no binding of the free dyes, labeled peptides, and small proteins to GroEL (6). Considering the very tight binding of rhodanese to GroEL, it seems improbable that the fluorophores have a strong effect on the interactions with the chaperone. [3] The remarkable promiscuity of GroEL/ES for different substrate proteins suggests that the chaperone will not be particularly sensitive to protein modifications. [4] We are directly comparing the folding kinetics of identically labeled proteins in free solution and inside the chaperonin cage.

Preparation of rhodanese-chaperone complexes. The ammonium sulfate precipitate of SR1 was resolubilized at 1 µM SR1 (heptamer) in folding buffer (50 mM TrisHCl (Roth), 10 mM $MgCl_2$ (Roth), 5 mM KCl (Roth), 100 mM 2-mercaptoethanol (Fluka Ultra), 0.001 % Tween 20 (Pierce), pH 7.5). Binding of rhodanese to SR1 was achieved by manually mixing 10 µl of 0.6 to 2 µM Rhodanese unfolded in 5 M GdmCl, 50 mM TrisHCl, 10 mM $MgCl_2$, 5 mM KCl, 100 mM 2-mercaptoethanol, 0.001 % Tween 20, pH 7.5 with 190 µl of a 1 µM solution of SR1 (heptamer). The complex was purified by size exclusion chromatography on a TSK 5000 PWXL column (TOSOH Bioscience) using fluorescence

detection. In the presence of 1 µM GroES and 2 mM ATP, the complexes of SR1-encapsulated rhodanese were stable for more than 100 min (Fig. S1).

Refolding experiments by manual mixing. Binary complexes of SR1 and rhodanese were prepared as described above. Chaperone-mediated refolding experiments were performed in folding buffer; they were initiated by the addition of GroES (final concentration 1 µM) and ATP (final concentration of 2 mM) to the SR1-rhodanese complexes. The spontaneous refolding reaction was observed by diluting rhodanese unfolded in 4 M GdmCl 100-fold into folding buffer. For experiments at different volume fractions of D_2O, the SR1-rhodanese complexes and unfolded rhodanese were incubated in folding buffer at the respective D_2O/H_2O mixture for 1 h before refolding was initiated. All solvent isotope exchange experiments were performed at 27 °C.

Fluorescence anisotropy measurements. Steady-state fluorescence anisotropy measurements were performed in folding buffer in a Fluorolog 3 fluorometer (HORIBA Jobin Yvon, Germany). Native encapsulated rhodanese was prepared by incubating the purified binary SR1-rhodanese complexes (size exclusion chromatography, PWXL column, TOSOH Bioscience) for 1h with 2 mM ATP and 1 µM GroES. The excitation and emission wavelengths were 488 nm and 515 nm for donor and 590 nm and 615 nm for acceptor anisotropy measurements, respectively. The excitation and emission slits were 5 nm, and an integration time of 1 s was used. In total, 60 data points were measured, and an average anisotropy was calculated from these values (Fig. S2).

Reactivation of rhodanese using an enzymatic assay (13). Binary complexes of SR1 with the L-variant of rhodanese were prepared by incubating 2 µM SR1 with 1 µM donor- and acceptor-labeled rhodanese in 50 µl folding buffer for 2h at 37°C. The binary complex was purified by size exclusion chromatography on a TSK 5000 PWXL column (TOSOH Bioscience). The concentration of rhodanese in this binary complex was 0.1 µM (according to the fluorescence of Alexa Fluor 594) in 500 µl folding buffer. A premix containing 0.05 M KCN, 0.04 M KH_2PO_4, and 0.05 M $Na_2S_2O_3$ was prepared. To trigger refolding, 2 mM ATP and 1 µM GroES were added to 100 µl of binary complex (27°C). After different times (0, 10, 15, 20, 25, 30, 40, 60, 80 min), 10 µl of the reaction were mixed with 1 µl of 0.5 M EDTA (pH7.3) and cooled on ice. 125 µl of the premix were added to the mixture, and the enzymatic reaction was allowed to proceed for 1 minute before stopping it by the addition of 62.5 µl 15% formaldehyde. To detect the product, SCN^-, 187.5 µl of a 6 % (w/v) $Fe(NO_3)_3$ solution in 12 % HNO_3 were added. The complexes of iron(III) with SCN^- were detected by their absorbance at 460 nm. Three independent replicates were used to determine the rate constant for reactivation (Fig. S11). Because of the very low rhodanese concentrations used in this experiment, a background reaction due to spontaneous refolding

of rhodanese during the dissociation of the complex on ice occurred. The background reaction was accounted for by repeating the reaction without the addition of GroES and ATP and subtracting it from the data. A single-exponential fit of the corrected data yielded a rate constant of 0.09 ± 0.04 min^{-1} (Fig. S11), within the range of rate constants (from ~0.04 min^{-1} to ~0.16 min^{-1}) reported in the literature for unlabeled rhodanese (14-17).

Limited proteolysis assay. Two singly-donor labeled variants (K135C-D and E285C-D) were used for limited proteolysis to probe the sequence of folding events in rhodanese (Fig. S10). Position K135C is located at the N-terminal end of the linker connecting the N- and C-terminal domains, whereas E285C is located in the C-terminal domain. The unfolded rhodanese variants (14 µM K135C-D and 7 µM E285C-D in 4 M GdmCl and folding buffer) were diluted (1:10) with folding buffer to a final volume of 200 µl. 100 seconds after starting the refolding reaction, 20 µl of a 20 mg/ml stock-solution of proteinase K were added. Proteolysis was stopped by mixing an aliquot of the reaction mixture (100 µl) with 10 µl 120% w/v TCA at 100 s and 300s after protease addition. The precipitate was dissolved in 50 µl SDS PAGE loading-buffer, and 10 µl were used for electrophoresis. The fluorescence of the attached Alexa Fluor 488 was measured in the gel (Fig. S10B) before staining with Coomassie brilliant blue R250 (Roth, Karlsruhe, Germany) (Fig. S10A). The fluorescence image (Fig. S10B, excitation wavelength 488 nm; Typhoon 9400, Amersham) shows a band with a mass of approximately 11 kD for variant E285C-D (fluorophore in the C-terminal domain), whereas only smaller fragments are observed for K135C-D (fluorophore in the N-terminal domain), suggesting that the C-terminal domain folds prior to the N-terminal domain. The molecular mass of the C-terminal domain (starting with Y163) is estimated to be 14 851 Da. Due to the high amount of protease used in the assay (2 mg/ml), no band of undigested rhodanese could be observed.

Single molecule measurements. Observations of single-molecule fluorescence were made using a MicroTime 200 confocal microscope (PicoQuant, Berlin, Germany) equipped with a 488 nm diode laser (Sapphire 488-100 CDRH, Coherent, Santa Clara, CA), a 80 MHz-pulsed laser (Optical Supercontinuum System SCF450-4-80MHz, Fianium, Southampton, UK), a 30 MHz-pulsed laser (Optical Supercontinuum System SCF450-4-30MHz Fianium), and an Olympus UplanApo 60x/1.20W objective. After passing through a 100 µm pinhole, sample fluorescence was separated first into parallel and perpendicular polarized light relative to the polarization of the exciting laser beam using a polarizing beam splitter cube. Afterwards, the two components were further separated into donor and acceptor components using a dichroic mirror (585DCXR, Chroma, Rockingham, VT). After passing two filters (Chroma ET525/50M, HQ650/100), each component was focused onto an avalanche photodiode (SPCM-AQR-15, PerkinElmer Optoelectronics, Vaudreuil, QC, Canada), and the arrival time of every detected photon was recorded using a

HydraHarp 400 counting card (PicoQuant, Berlin, Germany). All measurements were performed with laser powers of 70 µW to 100 µW. For dual color excitation of donor and acceptor (18, 19), the donor was excited continuously with a 488 nm diode laser (Sapphire 488-100 CDRH, Coherent, Santa Clara, CA) to maximize the excitation rate, and the acceptor was excited with picosecond pulses at a wavelength range selected by a z582/15 (Chroma) band pass filter and a pulse frequency of 30 MHz (Optical Supercontinuum Systems SCF450-4-30MHz Fianium, Southampton, UK). Successive photons detected in either channel and separated by less than 130 µs were combined into one burst. A burst was retained as a significant event if the total number of counts exceeded 20 (or 15 in case of the N-variant in the microfluidic mixer). Identified bursts were corrected for background, differences in quantum yields of donor and acceptor, the different collection efficiencies in the detection channels, cross-talk, and direct acceptor excitation as described previously (20). In addition, bursts during which acceptor photobleaching is likely to have occurred were discarded (6). A custom-built temperature-controlled sample holder employing peltier elements and a digital temperature controller (TC2812-LAB12, Cooltronic, Wil, Switzerland) with a PT100 platinum resistance temperature sensor (Minco EC AG, Wil, Switzerland) was used to adjust the temperature (21). The temperature in the confocal volume was determined via the temperature-dependent fluorescence lifetime of rhodamine B (RhB) (22) measured in a custom-built temperature-controlled ensemble time-correlated single photon counting instrument (23).

Data reduction by moving window analysis and singular value decomposition (SVD). For the moving window analysis, window sizes of Δt = 300 s (spontaneous folding of the N- and L-variant and SR1-mediated folding of N-, L-, and C-variant) or Δt = 50 s (spontaneous folding of the C-variant) were used. All bursts recorded within this window were used to obtain the following nine observables: transfer efficiency, burst duration, photon rate per burst (photon detection rate), donor fluorescence lifetime (parallel and perpendicular relative to the polarization of the excitation light), acceptor fluorescence lifetime (parallel and perpendicular to the polarization of the excitation light), donor anisotropy after donor excitation, and acceptor anisotropy after donor excitation. The observables were binned (25x25 bins) in two-dimensional histograms, with the transfer efficiency as one dimension. Bin-ranges were from E_{min} = -0.3 to E_{max} = 1.2 (transfer efficiency), t_{min} = 0 ms to t_{max} = 10 ms (burst duration), B_{min} = 0 ms^{-1} to B_{max} = 100 ms^{-1} (photon detection rate), r_{min} = -2 to r_{max} = 2 (anisotropy), and τ_{min} = 0 ns to τ_{max} = 8 ns (fluorescence lifetime). Every 2D-histogram was expressed column by column as a vector $\mathbf{a}_i(t_1)$ with 625 elements (25x25) for the first time window t_1. By arranging all sub-vectors $\mathbf{a}_i(t_1)$ in one vector $\mathbf{a}(t_1) = [\mathbf{a}_1(t_1), \mathbf{a}_2(t_1), \mathbf{a}_3(t_1),\ldots, \mathbf{a}_8(t_1)]$, the final vector (containing 5000 elements) for this time window (t_1) was obtained. The window was then shifted incrementally by $\Delta t/3$, and $\mathbf{a}(t_j)$ was calculated for the bursts resulting from every window

position. For the SVD, a time $t = t_s+\Delta t/2$ was assigned to every histogram, where t_s is the start time of the corresponding window. The procedure yields an $m \times n$ data matrix, **A,** with n vectors $\mathbf{a}(t_j)$ for n time points and m = 5000 bins of the nine observables.

SVD decomposes **A** into three matrices (**U**, **S** and **V**) (24):

$$\mathbf{A} = \mathbf{U}\,\mathbf{S}\,\mathbf{V}^{\mathbf{T}}. \qquad [S1]$$

Here, **U** is an $m \times m$ matrix of basis vectors (eigenvectors of $\mathbf{AA}^{\mathbf{T}}$), **S** is an $m \times n$ rectangular diagonal matrix whose elements give the weighting factors (or singular values) for every basis vector (the squared eigenvalues of $\mathbf{AA}^{\mathbf{T}}$ and $\mathbf{A}^{\mathbf{T}}\mathbf{A}$), and $\mathbf{V}^{\mathbf{T}}$ is a transposed $n \times n$ matrix of amplitude vectors (eigenvectors of $\mathbf{A}^{\mathbf{T}}\mathbf{A}$), describing the time course of the corresponding basis vectors. The number of nonzero diagonal elements of **S** that are necessary to reconstruct the data matrix from **U**, **S,** and **V** is an estimate of the number of distinguishable molecular species involved in the reaction mechanism. The two-dimensional representations of the first three basis vectors and the first three amplitude vectors for the spontaneous and SR1-mediated folding reaction of the N-variant, L-variant and C-variant are shown in Fig. S6, S7, S8 and S9, respectively. Raw data showing the first histograms immediately after starting the refolding reaction and the last histogram of the refolding reaction are shown for all three variants in Figs. S3, S4 and S5.

Microfluidic mixing experiments. For rapid mixing experiments, microfluidic mixers fabricated by replica molding in polydimethylsiloxane (PDMS) were used. For detecting the GroES-ATP-mediated encapsulation reaction of the SR1-bound rhodanese variants, the binary rhodanese-SR1 complex was mixed at a ratio of 1:5.7 with 2.4 µM GroES and 2.4 mM ATP, resulting in final concentrations of 2 µM GroES and 2 mM ATP. 0.01 % Tween 20 were included to prevent non-specific interactions of the chaperone-substrate complexes with the PDMS surfaces. Measurements were taken by placing the confocal volume at positions 75 µm (63 ms), 100 µm (94 ms), 200 µm (168 ms), 300 µm (252 ms), 600 µm (504 ms and 1.01 s), 900 µm (1.51 s), 1200 µm (2.02 s), and 1500 µm (2.52 s) downstream of the mixing region. To determine the transfer efficiency histogram at $t = 0$, the binary rhodanese-chaperone complex was measured 50 µm after the mixing region, without ATP and GroES in the side channels (Ch1 and Ch3, see Fig. 5A). The experiments were performed with pressures of 13.8 kPa (2.0 psi) applied to all channels for measurements from 50 µm (without GroES and ATP, 0 ms) to 600 µm (504 ms), and with 6.9 kPa (1.0 psi) for all measurements from 600 µm (1.01 s) to 1500 µm (2.52 s). The calculated flow velocities of 1.2 mm/s (13.8 kPa) and 0.6 mm/s (6.9 kPa) in the observation channel (Ch4) were used to convert distances to times as described by Pfeil *et al*. (25). The calculated velocities were confirmed by analyzing the donor-acceptor fluorescence intensity cross-correlation functions (26).

References

1. Quaite-Randall E & Joachimiak A (2000) Purification of GroES from an Overproducing E.coli Strain. *Methods Mol Biol* 140:41-49.
2. Kamireddi M, Eisenstein E, & Reddy P (1997) Stable expression and rapid purification of Escherichia coli GroEL and GroES chaperonins. *Protein Expr Purif* 11:47-52.
3. Horwich AL, Burston SG, Rye HS, Weissman JS, & Fenton WA (1998) Construction of single-ring and two-ring hybrid versions of bacterial chaperonin GroEL. *Methods Enzymol* 290:114-116.
4. Hoffmann A, Kane A, Nettels D, Hertzog DE, Baumgärtel P*, et al.* (2007) Mapping protein collapse with single-molecule fluorescence and kinetic synchrotron radiation circular dichroism spectroscopy. *Proc Natl Acad Sci USA* 104:105-110.
5. Nettels D, Gopich IV, Hoffmann A, & Schuler B (2007) Ultrafast dynamics of protein collapse from single-molecule photon statistics. *Proc Natl Acad Sci USA* 104:2655-2660.
6. Hillger F, Hänni D, Nettels D, Geister S, Grandin M*, et al.* (2008) Probing protein-chaperone interactions with single-molecule fluorescence spectroscopy. *Angew Chem Int Ed* 47:6184-6188.
7. Schuler B, Lipman EA, & Eaton WA (2002) Probing the free-energy surface for protein folding with single-molecule fluorescence spectroscopy. *Nature* 419:743-747.
8. Sherman E & Haran G (2006) Coil-globule transition in the denatured state of a small protein. *Proc Natl Acad Sci USA* 103:11539-11543.
9. Hofmann H, Golbik RP, Ott M, Hübner CG, & Ulbrich-Hofmann R (2008) Coulomb forces control the density of the collapsed unfolded state of barstar. *J Mol Biol* 376:597-605.
10. Tezuka-Kawakami T, Gell C, Brockwell DJ, Radford SE, & Smith DA (2006) Urea-induced unfolding of the immunity protein Im9 monitored by spFRET. *Biophys. J.* 91:L42-L44.
11. Merchant KA, Best RB, Louis JM, Gopich IV, & Eaton WA (2007) Characterizing the unfolded states of proteins using single-molecule FRET spectroscopy and molecular simulations. *Proc Natl Acad Sci USA* 104:1528-1533.
12. Margittai M, Widengren J, Schweinberger E, Schroder GF, Felekyan S*, et al.* (2003) Single-molecule fluorescence resonance energy transfer reveals a dynamic equilibrium between closed and open conformations of syntaxin 1. *Proc Natl Acad Sci USA* 100:15516-15521.
13. Tandon S & Horowitz PM (1989) Reversible folding of rhodanese. Presence of intermediate(s) at equilibrium. *J Biol Chem* 264:9859-9866.
14. Chaudhry C, Farr GW, Todd MJ, Rye HS, Brunger AT*, et al.* (2003) Role of the gamma-phosphate of ATP in triggering protein folding by GroEL-GroES: function, structure and energetics. *EMBO J* 22:4877-4887.
15. Weissman JS, Rye HS, Fenton WA, Beechem JM, & Horwich AL (1996) Characterization of the active intermediate of a GroEL-GroES-mediated protein folding reaction. *Cell* 84:481-490.
16. Tang Y, Chang H, Chakraborty K, Hartl F, & Hayer-Hartl M (2008) Essential role of the chaperonin folding compartment in vivo. *EMBO J.*

17. Farr GW, Fenton WA, & Horwich AL (2007) Perturbed ATPase activity and not "close confinement" of substrate in the cis cavity affects rates of folding by tail-multiplied GroEL. *Proc Natl Acad Sci USA* 104:5342-5347.
18. Müller BK, Zaychikov E, Bräuchle C, & Lamb DC (2005) Pulsed interleaved excitation. *Biophys. J.* 89:3508-3522.
19. Kapanidis AN, Lee NK, Laurence TA, Doose S, Margeat E*, et al.* (2004) Fluorescence-aided molecule sorting: analysis of structure and interactions by alternating-laser excitation of single molecules. *Proc Natl Acad Sci USA* 101:8936-8941.
20. Schuler B (2007) Application of single molecule Förster resonance energy transfer to protein folding. *Methods Mol Biol* 350:115-138.
21. Nettels D, Müller-Späth S, Küster F, Hofmann H, Haenni D*, et al.* (2009) Single-molecule spectroscopy of the temperature-induced collapse of unfolded proteins. *Proc Natl Acad Sci USA*.
22. Benninger RK, Koç Y, Hofmann O, Requejo-Isidro J, Neil MA*, et al.* (2006) Quantitative 3D mapping of fluidic temperatures within microchannel networks using fluorescence lifetime imaging. *Anal Chem* 78:2272-2278.
23. Nettels D, Hoffmann A, & Schuler B (2008) Unfolded Protein and Peptide Dynamics Investigated with Single-Molecule FRET and Correlation Spectroscopy from Picoseconds to Seconds. *J Phys Chem B*.
24. Henry E & Hofrichter J (1992) Singular value decomposition - Application to analysis of experimental data. *Methods Enzymol* 210:129-192.
25. Pfeil SH, Wickersham CE, Hoffmann A, & Lipman EA (2009) A microfluidic mixing system for single-molecule measurements. *Rev Sci Instrum* 80:055105.
26. Gösch M, Blom H, Holm J, & Rigler R (2000) Hydrodynamic flow profiling in microchannel structures by single molecule fluorescence spectroscopy. *Anal Chem* 72:3260-3265.
27. Hillger F, Nettels D, Dorsch S, & Schuler B (2007) Detection and analysis of protein aggregation with confocal single molecule fluorescence spectroscopy. *J Fluoresc* 17:759-765.

Supporting Figures

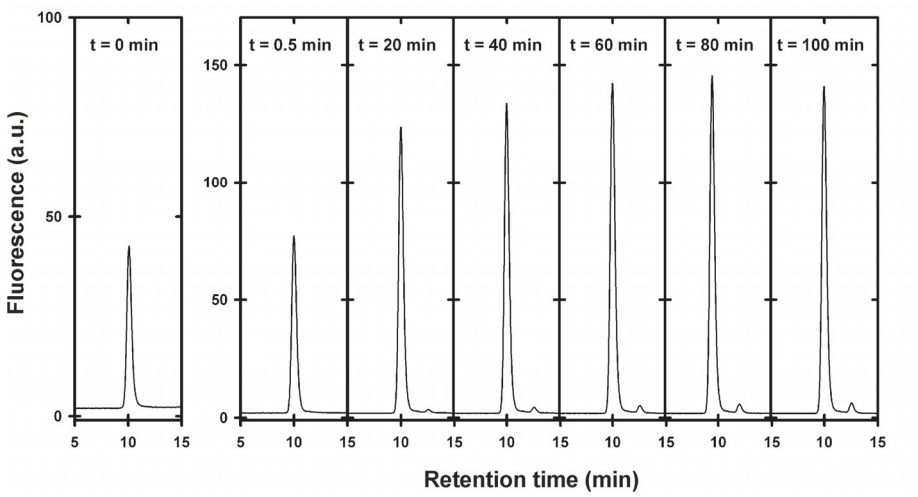

Fig. S1. Stability of the SR1-rhodanese-GroES complex. Elution profiles of analytical size exclusion chromatography of the rhodanese-SR1 complex (using singly acceptor-labeled rhodanese K135C) are shown at different times *t* after starting the refolding reaction by adding 1 μM GroES and 2 mM ATP. A TSK 5000 PWXL column (TOSOH Bioscience) with a flow rate of 0.8 ml/min and fluorescence detection was used (excitation at 585 nm, emission at 610 nm). The profile at $t = 0$ min is the size exclusion chromatography run before adding GroES and ATP. The peak at a retention time of 10 min corresponds to the chaperonin-rhodanese complex. Only very small amounts of free rhodanese (peak at 12.5 min) form over the course of the experiment. The increase in fluorescence of the peak corresponding to the chaperonin-rhodanese complex reflects the folding reaction inside the chaperonin cavity. The experiment was performed in folding buffer at room temperature.

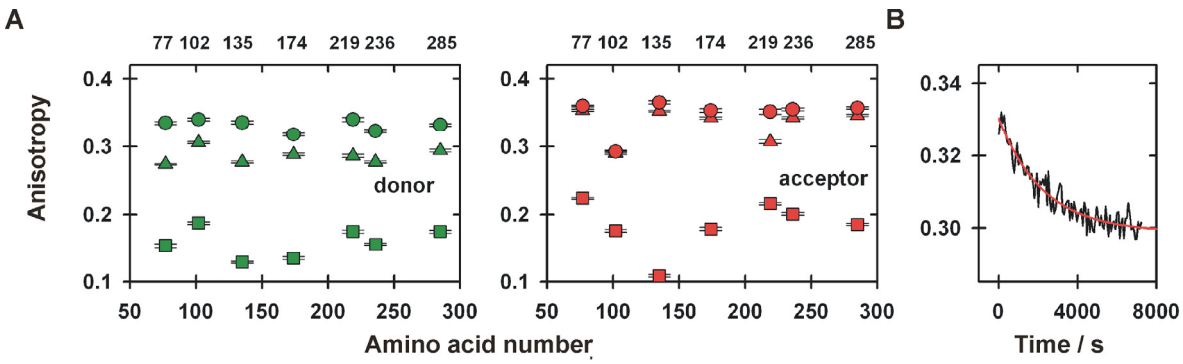

Fig. S2. Steady-state anisotropy measurements. (**A**) Single-cysteine variants of rhodanese were labeled either with the donor (green) or with the acceptor dye (red). Anisotropy values were recorded for free rhodanese (squares), binary rhodanese-SR1 complex (circles), and the encapsulated native rhodanese (triangles). (**B**) Kinetics of the change in donor anisotropy of the singly donor-labeled rhodanese variant K174C after addition of 1 µM GroES and 2 mM ATP at 22°C. The single exponential fit (solid line) yields a rate constant of $(4 \pm 1)\cdot 10^{-4}$ s^{-1}. The good agreement with the rate constants obtained from the single-molecule FRET experiments on doubly labeled protein [$(3.2 \pm 1.3)\cdot 10^{-4}$ s^{-1} for the N-variant and $(3.0 \pm 0.5)\cdot 10^{-4}$ s^{-1} for the L-variant at 22°C] supports the accuracy of the single molecule results and provides some indication that dye labeling does not affect the kinetics significantly (at least for AlexaFluor594, which is the larger chromophore). All measurements were performed in folding buffer.

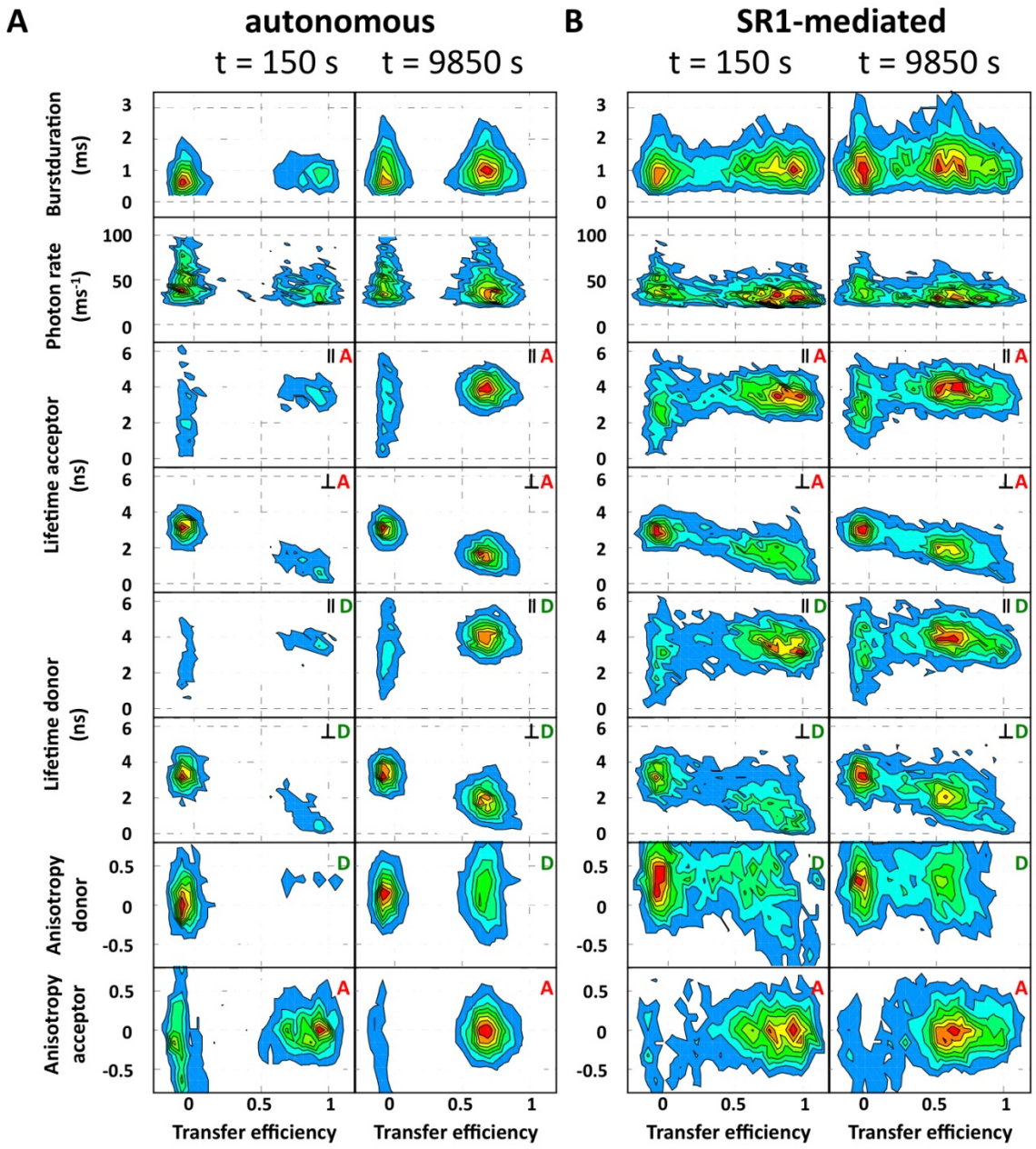

Fig. S3. 2D-Histograms for the autonomous **(A)** and SR1-mediated **(B)** folding reaction of the N-variant at the earliest (left) and latest (right) time point after starting the refolding reaction at 24°C.

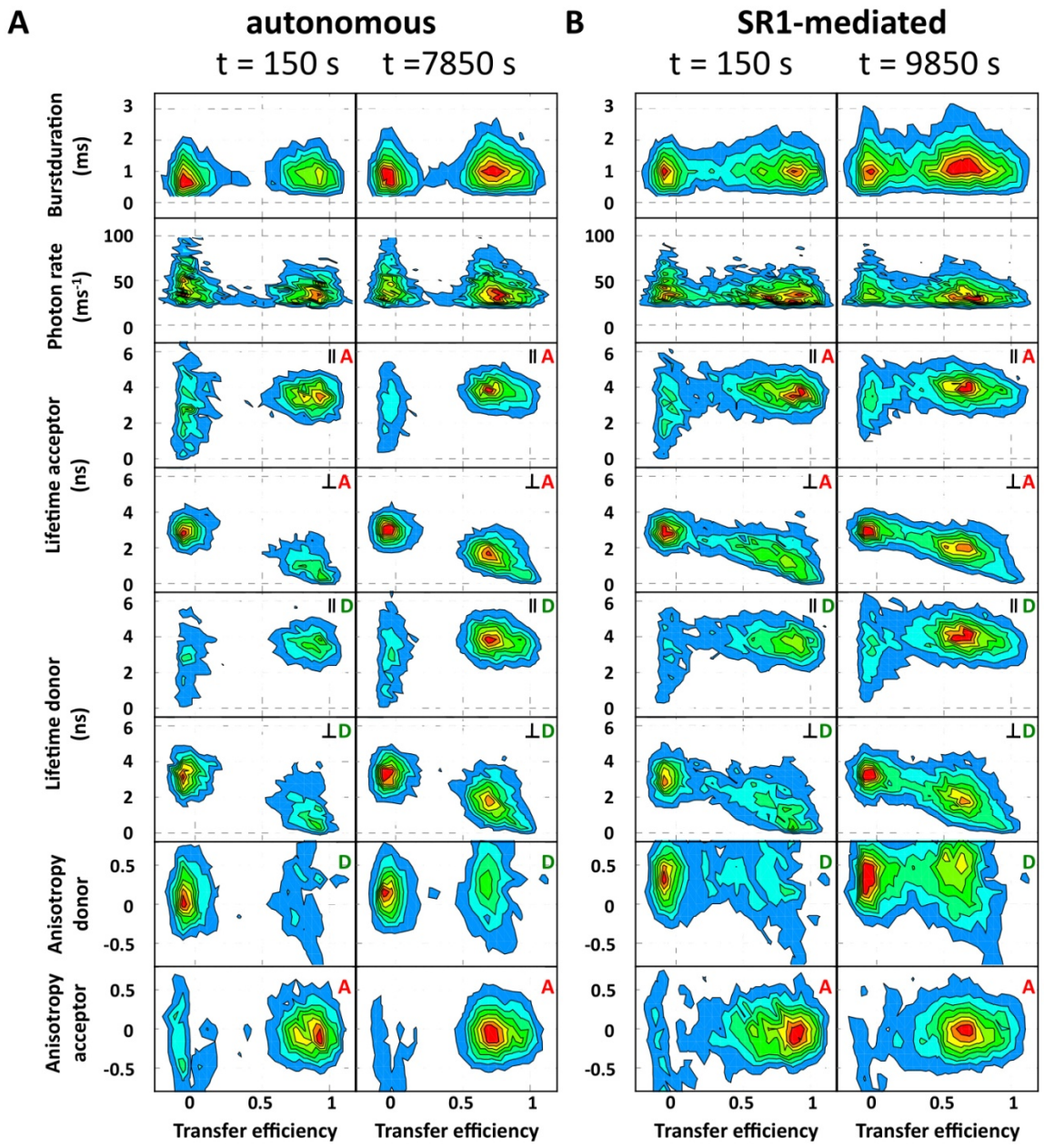

Fig. S4. 2D-Histograms for the autonomous **(A)** and SR1-mediated **(B)** folding reaction of the L-variant at the earliest (left) and latest (right) time point after starting the refolding reaction at 24°C.

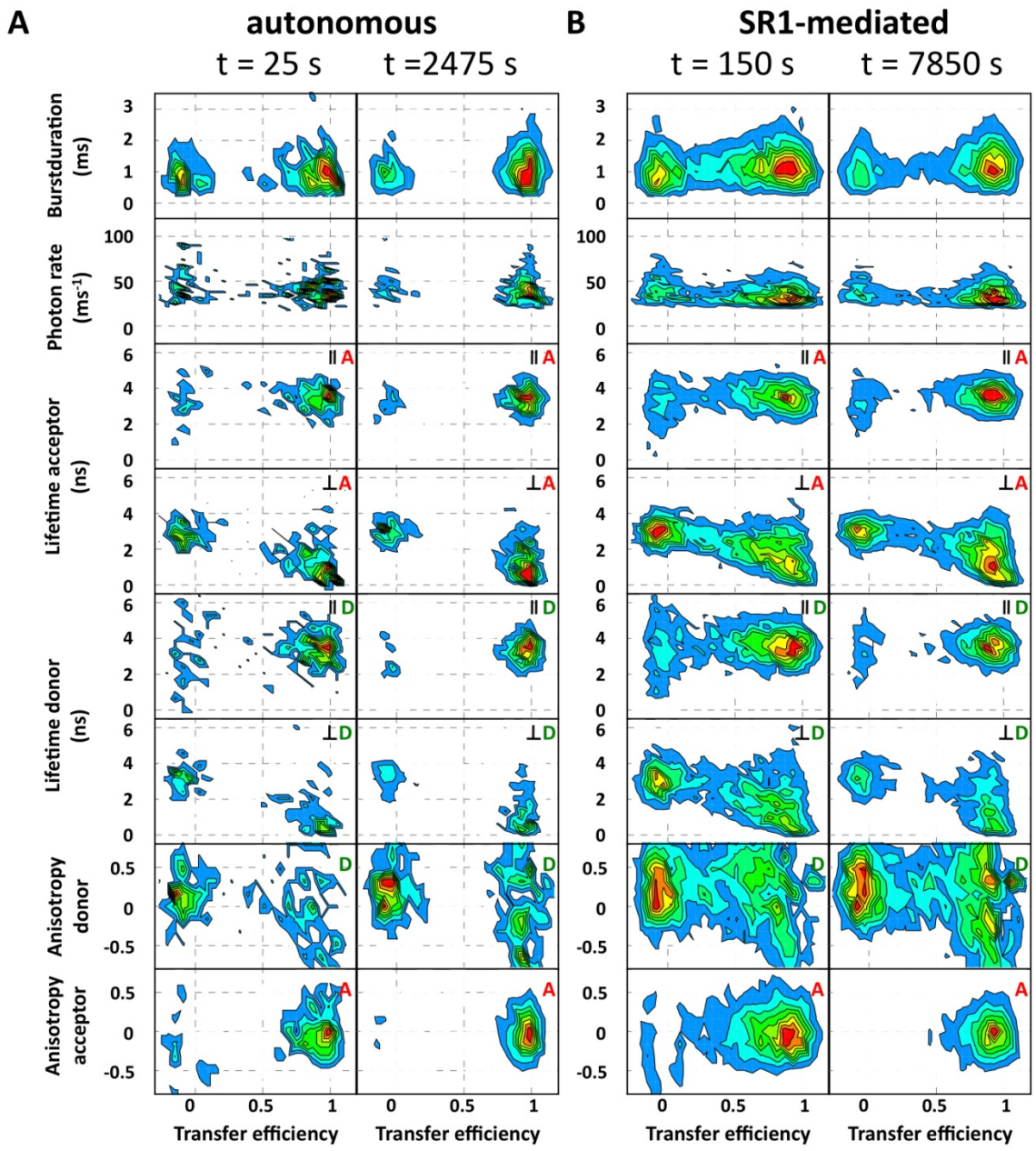

Fig. S5. 2D-Histograms for the autonomous **(A)** and SR1-mediated **(B)** folding reaction of the C-variant at the earliest (left) and latest (right) time point after starting the refolding reaction at 24°C.

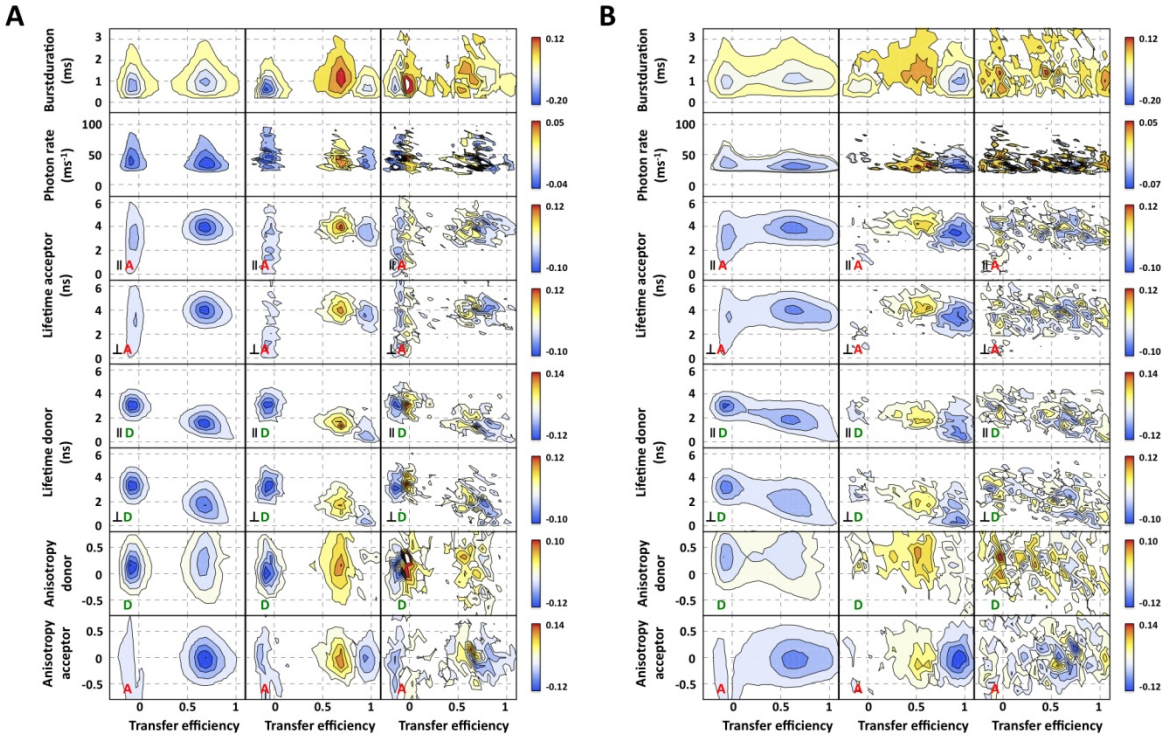

Fig. S6. Two-dimensional basis vectors of the multi-dimensional SVD for the spontaneous **(A)** and SR1-mediated **(B)** folding reaction of the N-variant at 24°C. The basis vectors indicate the positions of changes in the histograms of the corresponding observables (from top to bottom) and are ordered according to their singular values (from left to right). Basis vector 1 (left panel) describes an increase in the number of molecules during refolding. Basis vector 2 (middle panel) describes the conversion of the signature of non-native molecules (blue) to that of the native state (yellow and red). The larger noise level of basis vector 3 and the small corresponding singular values (see Fig. S9) for both the spontaneous (A) and the SR1-mediated folding reaction (B) indicate that the folding reaction is dominated by two distinguishable molecular species. The color code reflects the absolute SVD amplitude (see color scale).

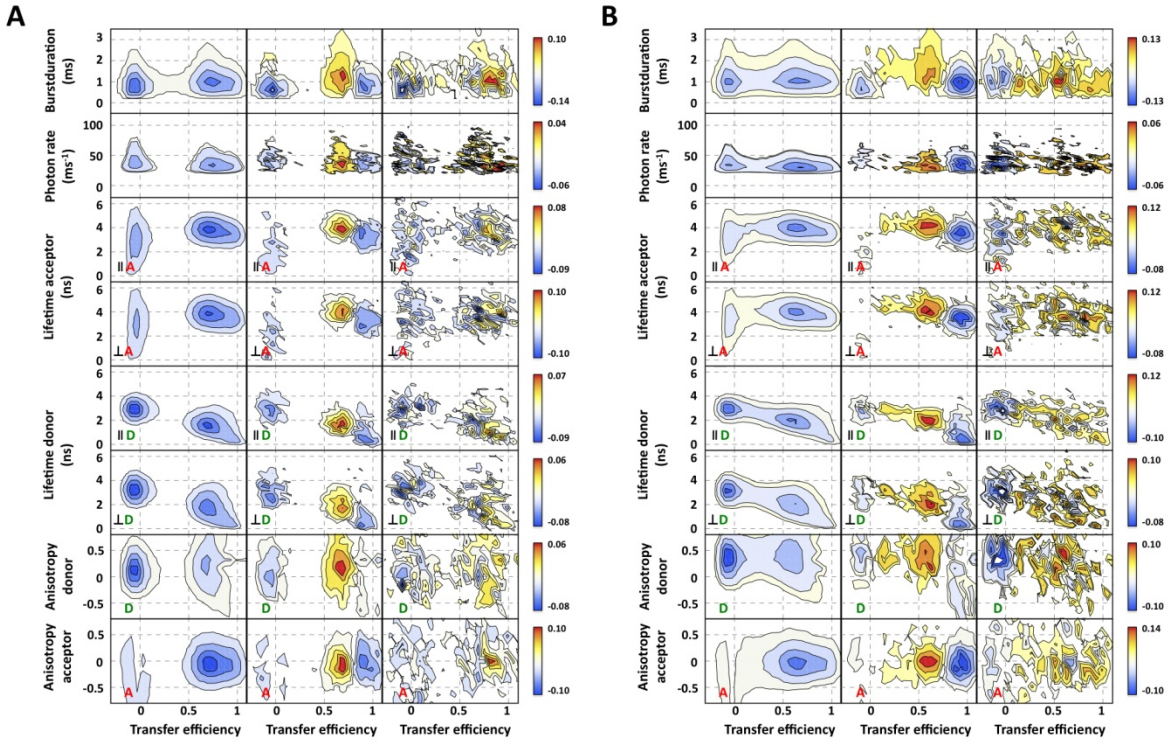

Fig. S7. Two-dimensional basis vectors of the multi-dimensional SVD for the spontaneous **(A)** and SR1-mediated **(B)** folding reaction of the L-variant at 24°C. The basis vectors indicate the positions of changes in the histograms of the corresponding observables (from top to bottom) and are ordered according to their singular values (from left to right). Basis vector 1 (left panel) describes an increase in the number of molecules during refolding. Basis vector 2 (middle panel) describes the conversion of the signature of non-native molecules (blue) to that of the native state (yellow and red). The larger noise level of basis vector 3 and the small corresponding singular values (see Fig. S9) for both the spontaneous (A) and the SR1-mediated folding reaction (B) indicate that the folding reaction is dominated by two distinguishable molecular species. The color code reflects the absolute SVD amplitude (see color scale).

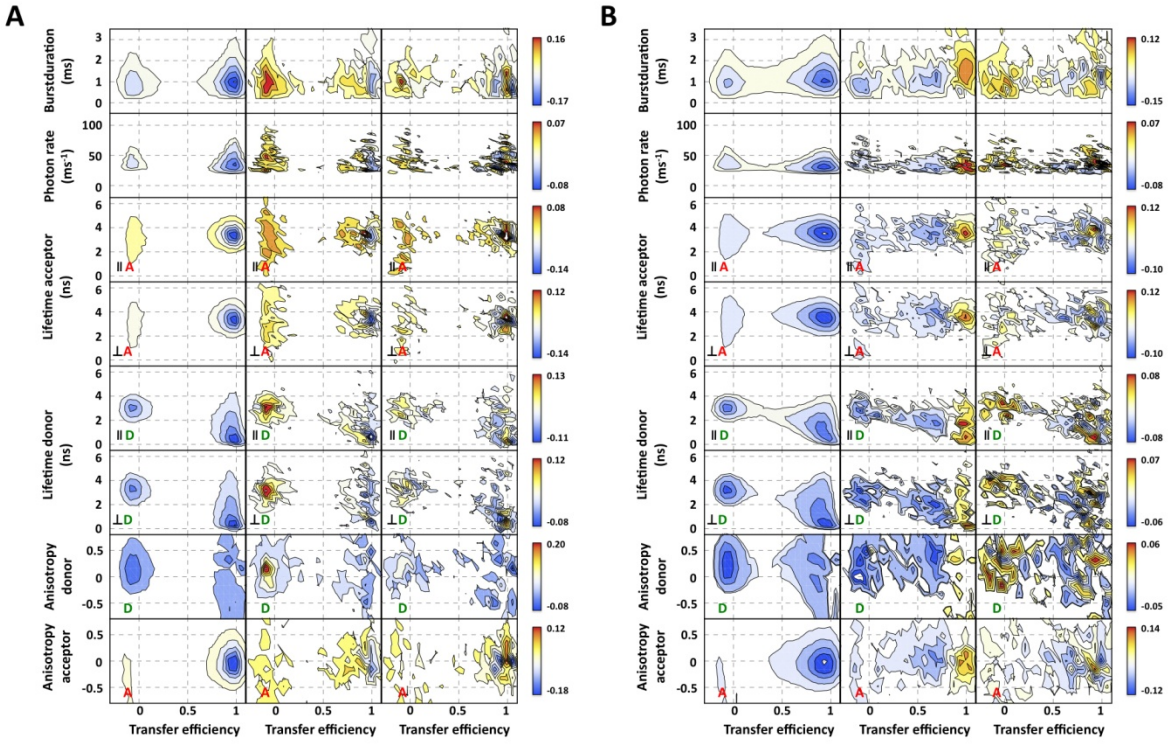

Fig. S8. Two-dimensional basis vectors of the multi-dimensional SVD for the spontaneous **(A)** and SR1-mediated **(B)** folding reaction of the C-variant at 24°C. The basis vectors indicate the position of a change in the histogram of the corresponding observable (from top to bottom) and are ordered according to their singular values (from left to right). Basis vector 1 (left panel) describes an increase in the number of molecules during refolding. Basis vector 2 (middle panel) describes the conversion of the signature of non-native molecules (blue) to that of the native state (yellow and red). The larger noise level of basis vector 3 and the small corresponding singular values (see Fig. S9) for both the spontaneous (A) and the SR1-mediated folding reaction (B) indicate that the folding reaction is dominated by two distinguishable molecular species. The color code reflects the absolute SVD amplitude (see color scale).

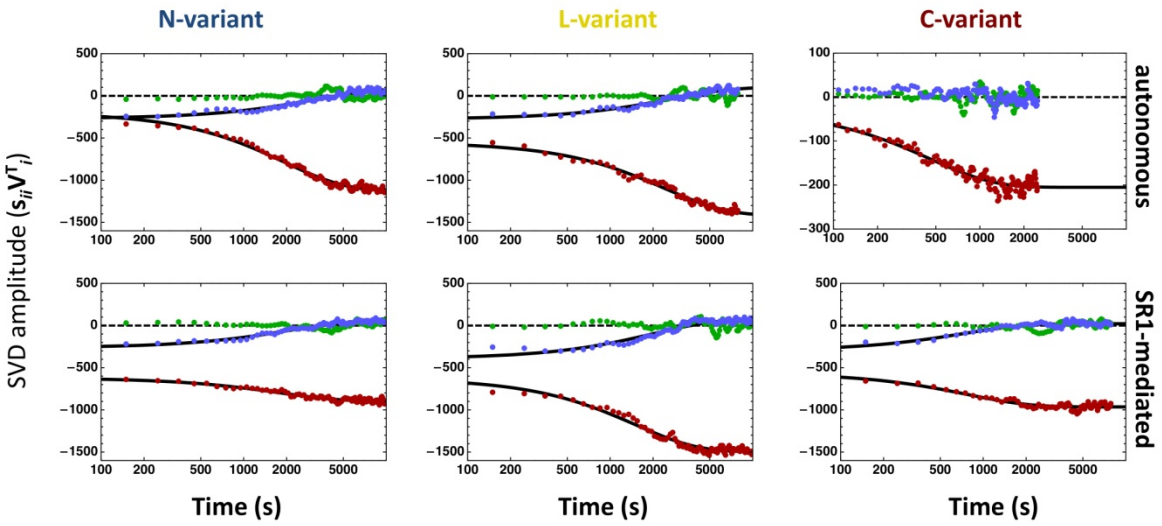

Fig. S9. First (red), second (blue), and third (green) amplitude vector weighted by their corresponding singular values (s_{ii}) of the multi-dimensional SVD for the spontaneous (upper panels) and SR1-mediated (lower panels) folding reaction of the N-, L-, and C-variants at 24°C. The first two amplitude vectors dominate the observed signal change.

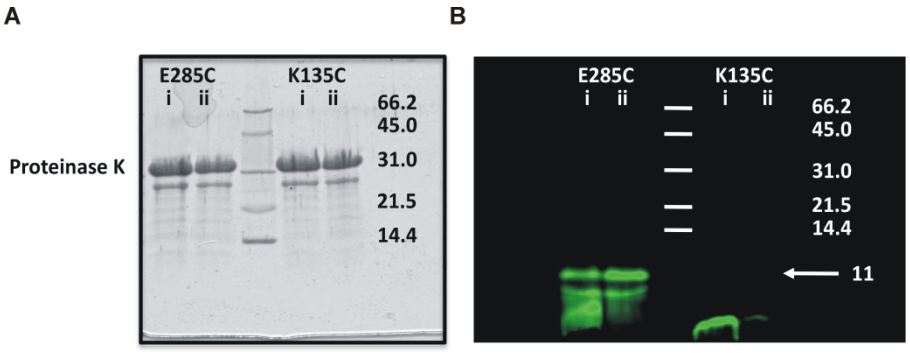

Fig. S10. Limited Proteolysis of singly-labeled rhodanese (K135C-D and E285C-D) indicates that the C-terminal domain folds prior to the N-terminal domain. **(A)** Coomassie stained SDS-Polyacrylamide gel (17%) of the proteolysis reaction mixture stopped at 100 s (i) and 300 s (ii) after addition of 2 mg/ml proteinase K. **(B)** Same gel, but scanned with an excitation wavelength of 488 nm.

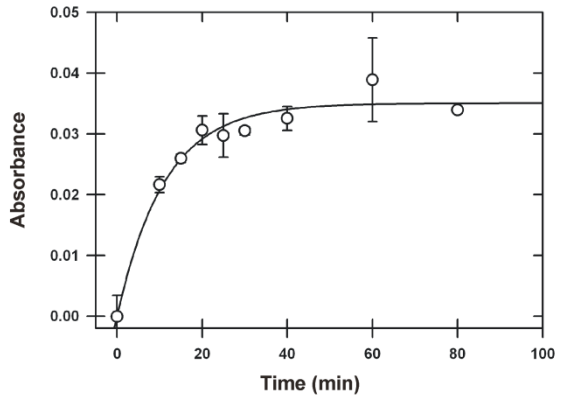

Fig. S11. Reactivation of doubly labeled rhodanese K135C/K174C by SR1. Enzymatic test as described in the supporting text. Error bars show standard errors of the means resulting from 3 independent measurements. A single-exponential fit yields a rate constant of 0.09 ± 0.04 min^{-1}, within the range of rate constants (from ~0.04 min^{-1} to ~0.16 min^{-1}) reported in the literature (14-17). The reactivation kinetics agree well with our single molecule results, especially considering the spread of previously reported values, the lack of temperature control for some of them, and the slow GroEL/ES dissociation step on ice required prior to the enzymatic test (13).

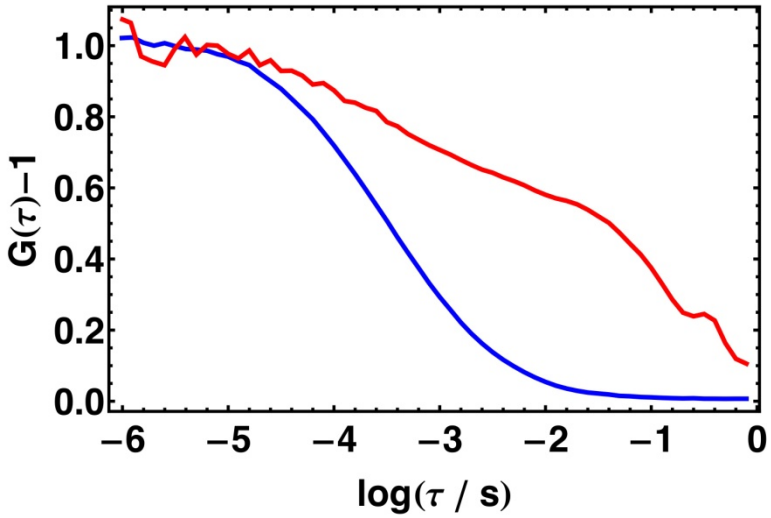

Fig. S12. Monitoring aggregation in single molecule experiments with fluorescence correlation spectroscopy. Under the experimental conditions and picomolar protein concentrations used in this work, no aggregation of rhodanese occurred, as illustrated by the normalized donor-acceptor fluorescence intensity cross-correlation function of the L-variant after initiation of refolding by manual mixing at 24°C (blue). The signatures of aggregated rhodanese previously observed in fluorescence lifetimes and burst size distributions (27) were also absent under these conditions. For comparison, a normalized cross-correlation function of rhodanese L-variant in the presence of an excess of unlabeled wildtype rhodanese is shown in red. The sample containing 4 nM labeled L-variant and 3 μM rhodanese wildtype was incubated for 2 minutes in 3 M urea. After dilution 1:50 into native conditions, the single molecule fluorescence time trace was recorded and the cross-correlation function calculated. The presence of aggregates leads to a heterogeneous distribution of translational diffusion times through the confocal volume and a correspondingly slower and in some cases even non-monotonic decay of the correlation function.